Simplified nonlinear theory of the dielectric loaded rectangular Cerenkov maser*

Zhao Ding(赵 鼎)† and Ding Yao-Gen(丁耀根)

Key Laboratory of High Power Microwave Sources and Technologies, Institute of Electronics, Chinese Academy of Sciences, Beijing 100190, *China*

(Received 28 December 2011; revised manuscript received 23 February 2012)

To rapidly and accurately investigate the performance of the dielectric loaded rectangular Cerenkov maser, a simplified nonlinear theory is proposed, in which the variations of wave amplitude and wave phase are determined by two coupled first-order differential equations. Through combining with the relativistic equation of motion and adopting the forward wave assumption, the evolutions of the forward wave power, the power growth rate, the axial wave number, the accumulated phase offset, and the information of the particle movement can be obtained in a single-pass calculation. For an illustrative example, this method is used to study the influences of the beam current, the gap distance between the beam and the dielectric surface, and the momentum spread on the forward wave. The variations of the saturated power and the saturation length with the working frequency for the beams with different momentum spreads have also been studied. The result shows that the beam–wave interaction is very sensitive to the electron beam state. To further verify this simplified theory, a comparison with the result produced from a rigorous method is also provided, we find that the evolution curves of the forward wave power predicted by the two methods exhibit excellent agreement. In practical applications, the developed theory can be used for the design and analysis of the rectangular Cerenkov maser.

Keywords: Cerenkov maser, dielectric load, rectangular waveguide, nonlinear theory

PACS: 41.60.Bq, 41.20.Jb, 84.40.Ik, 94.05.Pt **DOI:** 10.1088/1674-1056/21/9/094102

1. Introduction

When a charged particle moves through a medium with a constant velocity that is greater than the speed of light in the medium, the electromagnetic radiation will be generated. This phenomenon was firstly studied by a soviet physicist Cerenkov in 1934,[1] thereafter, it was called the Cerenkov radiation to commemorate the pioneer researcher. In 1947, another soviet physicist Ginzburg put forward a suggestion that the Cerenkov effect could be used to produce radio waves in the microwave regime.[2] From then on, a number of theoretical and experimental works on the Cerenkov maser have been done by different researchers all over the world.

Through using a rectilinear electron beam interacting with a dielectric loaded waveguide, the Cerenkov maser has the potential to generate the electromagnetic radiation from the microwave to the terahertz regime.[3−12] Compared with the free electron lasers and the gyrotrons, the dielectric loaded Cerenkov maser is intrinsically simple and compact; meanwhile, it can effectively produce millimeter or sub-millimeter waves with the characteristics of high power and broadband tunable ability, all of which make the Cerenkov maser possible to be used in wide applications, for instance, plasma diagnostics, spectroscopy, advanced radar, and communication system.

In the cylindrical Cerenkov maser, a hollow electron beam is injected to pass through a cylindrical waveguide with a dielectric liner. In the process, the electrons gradually lose their kinetic momenta, and the electromagnetic field of the working mode grows up correspondingly. With the development of the sheet beam technology, the dielectric loaded rectangular waveguide can be used as a new interaction circuit. In comparison with the traditional cylindrical structure, it has the following advantages. Firstly, the output power level in the millimeter or sub-millimeter wave regime can be improved by the prominent increases of the beam current and the interaction area, which are due to the introduction of the plane structure with a large transverse dimension. Moreover, since the space charge force in the sheet beam can be kept at a lower value, the electron momentum spread

*Project supported by the National Natural Science Foundation of China (Grant No. 60801031).

†Corresponding author. E-mail: dzhao@mail.ie.ac.cn

© 2012 Chinese Physical Society and IOP Publishing Ltd

can be lessened to reduce the adverse effects on the beam–wave interaction. In addition, the hybrid slow-wave mode in the dielectric loaded regime can be directly and smoothly converted to the linear polarized fast-wave mode by using a dielectric taper in the rectangular waveguide.[13]

In the past, theoretical investigations on the Cerenkov masers mainly focused on the linear characteristics of the cylindrical cases.[14−18] However, in recent years, the studies on the interaction system involved with the sheet beam and the dielectric loaded waveguide gradually attracted more attention. By using the kinetic theory, a dispersion relation for the Cerenkov instability in a dielectric loaded parallel plate waveguide sheet beam system has been rigorously derived.[19] For a real dielectric loaded rectangular waveguide with a sheet beam, an approximate dispersion relation to describe the three-dimensional beam–wave interaction has also been obtained.[11,20] The linear theory can accurately predict the linear growth rate, bandwidth, initial power gain, and other small signal characteristics in the interaction process.

For a real Cerenkov maser, the output power cannot keep increasing forever, it will attain a saturated value in a limited length. The real state of the electron beam also has obvious influences on the device performances. To better understand the characteristics in this physical system, a complete nonlinear analysis is necessary. In Ref. [21], a three-order differential equation of the field-evolution function has been found. By combining this equation with the relativistic equation of motion and applying the traveling-wave boundary condition, the beam–wave interaction can be self-consistently determined through numerical calculations. This method is rigorous enough in mathematics, but has the drawback of time consuming. To perform a rapid nonlinear analysis on the Cerenkov maser, we can describe the variations of wave amplitude and phase separately by using two coupled first-order differential equations, which is like that presented in Ref. [22]. At the same time, the boundary condition merely adopts the forward-wave assumption. The validation of this simplified nonlinear theory can be verified through comparing with the results from the rigorous method in Ref. [21].

In this paper, the theoretical model for the nonlinear interaction between the sheet beam and the dielectric loaded rectangular waveguide is presented in Section 2. For a demonstrative example, numerical results are given in Section 3, where the effect of the electron momentum spread is studied, and the validation check of the simplified nonlinear theory is also provided. Section 4 gives a brief summary.

2. Theoretical model

The dielectric loaded rectangular waveguide sheet beam interaction system is shown in Fig. 1, where a tenuous sheet beam with transverse dimension L is confined by a strong uniform magnetic field B_0 and propagates along the z axis direction. In the rectangular waveguide with width a, the thickness of the dielectric layer is d, and the height of the vacuum region is b. The sheet beam is above but near the dielectric layer in order to effectively interact with the surface wave.

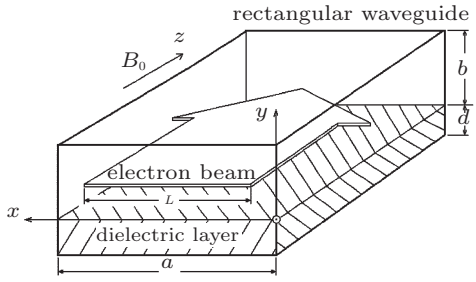


Fig. 1. Diagram of three-dimensional dielectric loaded rectangular waveguide sheet beam interaction system.

By choosing E_y as the potential function and using the Maxwell equations, the nonzero components of the slow wave mode EH_{mn} (E_z is dominant over H_z) can be written as

$$E_y = A\cos\left[\kappa_d\left(y+d\right)\right]\sin\left(k_x x\right)\,\mathrm{e}^{\mathrm{i}\alpha},\quad -d<y<0, \tag{1}$$

$$E_y = B\cosh\left[\kappa_0\left(b-y\right)\right]\sin\left(k_x x\right)\,\mathrm{e}^{\mathrm{i}\alpha},\quad 0\le y<b, \tag{2}$$

$$E_x = \frac{1}{k_x^2+k_z^2}\frac{\partial^2 E_y}{\partial y\partial x},\quad E_z = \frac{1}{k_x^2+k_z^2}\frac{\partial^2 E_y}{\partial y\partial z},$$
$$H_x = \frac{\mathrm{i}\omega\varepsilon}{k_x^2+k_z^2}\frac{\partial E_y}{\partial z},\quad H_z = \frac{-\mathrm{i}\omega\varepsilon}{k_x^2+k_z^2}\frac{\partial E_y}{\partial x}, \tag{3}$$

where $k_x = m\pi/a$, $m = 1, 2, \ldots$ for the EH_{mn} modes, ε is the permittivity of the two regions, ω and k_z are the angular frequency and the axial wave number, respectively, $\kappa_d^2 = \varepsilon_{\mathrm{r}}\omega^2/c^2 - k_x^2 - k_z^2$, and $\kappa_0^2 = k_x^2 + k_z^2 - \omega^2/c^2$, with c being the speed of light in vacuum and ε_{r} being the relative permittivity in the dielectric regime. The phase of the EH_{mn} mode is defined as

$$\alpha = \int_0^z k_z\left(z'\right)\mathrm{d}z' - \omega t. \tag{4}$$

In the above expressions, axial wave number k_z and amplitudes A and B are all real numbers and slowly vary along the z axis. For the cold-state dielectric loaded waveguide, there exists the following dispersion relation:

$$\kappa_d \tan \kappa_d d = \varepsilon_{\rm r} \kappa_0 \tanh \kappa_0 b, \tag{5}$$

and amplitudes A and B can be related through the equation

$$B = \varepsilon_{\rm r} \frac{\cos \kappa_d d}{\cosh \kappa_0 b} A. \tag{6}$$

In the vacuum region, the real part of H_x can be substituted in the following expression:

$$\left(\frac{\omega^2}{c^2} - k_x^2 + \kappa_0^2 + \frac{\partial^2}{\partial z^2} \right) H_x = - \left(\frac{\partial J_z}{\partial y} - \frac{\partial J_y}{\partial z} \right). \tag{7}$$

For the algebraic operation of H_x, the second-order derivatives of amplitude A (according to Eq. (6), amplitude B is substituted by A) and phase α are omitted under the assumption of slow variation.

After expanding Eq. (7), we have

$$\begin{aligned} &\frac{\omega \varepsilon_0 \varepsilon_{\rm r} k_z}{k_x^2 + k_z^2} \frac{\cos \kappa_d d}{\cosh \kappa_0 b} \cosh \left[\kappa_0 (b - y) \right] \sin (k_x x) \\ &\quad \times \left[\left(\frac{\omega^2}{c^2} - k_x^2 - k_z^2 + \kappa_0^2 \right) A \cos \alpha - 2 k_z \frac{{\rm d}A}{{\rm d}z} \sin \alpha \right] \\ &= \frac{\partial J_z}{\partial y} - \frac{\partial J_y}{\partial z}, \end{aligned} \tag{8}$$

where ε_0 is the permittivity in vacuum, and J_y and J_z represent the y- and the z-directional electron currents, respectively.

In the dielectric region, the real part of H_x can be substituted into the simplified source-free equation

$$\left(\varepsilon_{\rm r} \frac{\omega^2}{c^2} - k_x^2 - \kappa_d^2 + \frac{\partial^2}{\partial z^2} \right) H_x = 0. \tag{9}$$

After a series of derivations, we obtain

$$\begin{aligned} &\frac{\omega \varepsilon_0 \varepsilon_{\rm r} k_z}{k_x^2 + k_z^2} \cos \left[\kappa_d (y + d) \right] \sin (k_x x) \\ &\quad \times \left[\left(\varepsilon_{\rm r} \frac{\omega^2}{c^2} - k_x^2 - k_z^2 - \kappa_d^2 \right) A \cos \alpha \right. \\ &\quad \left. - 2 k_z \frac{{\rm d}A}{{\rm d}z} \sin \alpha \right] = 0, \end{aligned} \tag{10}$$

where the relationship $\varepsilon_{\rm r} \omega^2 / c^2 - k_x^2 - k_z^2 - \kappa_d^2 = \omega^2 / c^2 - k_x^2 - k_z^2 + \kappa_0^2$ can be introduced to unify the equations for the two regions.

On the transverse section of the rectangular waveguide, the Poynting energy integral is a constant

$$\begin{aligned} \frac{1}{A^2} \int H_x E_y^* {\rm d}s = \frac{1}{2} \frac{a \omega \varepsilon_0 \varepsilon_{\rm r} k_z}{k_x^2 + k_z^2} \frac{1}{\cosh^2 \kappa_0 b} \\ \times \left[\cosh^2 \kappa_0 b \left(\frac{d}{2} + \frac{\sin 2 \kappa_d d}{4 \kappa_d} \right) \right. \\ \left. + \varepsilon_{\rm r} \cos^2 \kappa_d d \left(\frac{b}{2} + \frac{\sinh 2 \kappa_0 b}{4 \kappa_0} \right) \right]. \end{aligned} \tag{11}$$

Combining Eqs. (8), (10), and (11), we can obtain the following expression:

$$\begin{aligned} &\left(\frac{\omega^2}{c^2} - k_x^2 - k_z^2 + \kappa_0^2 \right) A \cos \alpha - 2 k_z \frac{{\rm d}A}{{\rm d}z} \sin \alpha \\ &= \frac{1}{C_{mn}} \int_0^b \int_0^a \cosh \left[\kappa_0 (b - y) \right] \sin (k_x x) \\ &\quad \times \left(\frac{\partial J_z}{\partial y} - \frac{\partial J_y}{\partial z} \right) {\rm d}x {\rm d}y, \end{aligned} \tag{12}$$

where

$$\begin{aligned} C_{mn} = \frac{1}{2} \frac{a \omega \varepsilon_0 k_z}{k_x^2 + k_z^2} \left[\frac{\cosh \kappa_0 b}{\cos \kappa_d d} \left(\frac{d}{2} + \frac{\sin 2 \kappa_d d}{4 \kappa_d} \right) \right. \\ \left. + \varepsilon_{\rm r} \frac{\cos \kappa_d d}{\cosh \kappa_0 b} \left(\frac{b}{2} + \frac{\sinh 2 \kappa_0 b}{4 \kappa_0} \right) \right]. \end{aligned} \tag{13}$$

Through separately multiplying both sides of Eq. (12) with $\cos \alpha$ and $\sin \alpha$, and then averaging them in one time period, the following two equations can be obtained:

$$\begin{aligned} &\left(\frac{\omega^2}{c^2} - k_x^2 - k_z^2 + \kappa_0^2 \right) A \\ &= \frac{\omega}{\pi C_{mn}} \int_0^{2\pi/\omega} {\rm d}t \int_0^a \sin (k_x x) \, {\rm d}x \int_0^b {\rm d}y \\ &\quad \times \left\{ \kappa_0 \sinh \left[\kappa_0 (b - y) \right] J_z \cos \alpha \right. \\ &\quad \left. - k_z \cosh \left[\kappa_0 (b - y) \right] J_y \sin \alpha \right\}, \\ &\quad -2 k_z \frac{{\rm d}A}{{\rm d}z} \end{aligned} \tag{14}$$

$$\begin{aligned} &= \frac{\omega}{\pi C_{mn}} \int_0^{2\pi/\omega} {\rm d}t \int_0^a \sin (k_x x) \, {\rm d}x \int_0^b {\rm d}y \\ &\quad \times \left\{ \kappa_0 \sinh \left[\kappa_0 (b - y) \right] J_z \sin \alpha \right. \\ &\quad \left. + k_z \cosh \left[\kappa_0 (b - y) \right] J_y \cos \alpha \right\}. \end{aligned} \tag{15}$$

In the deduction of the above equations, it should be noted that the slowly varying physical variable exhibits an equivalent change when it evolves over one time period or travels through one axial wavelength in a steady state system. For the beam current density, there is an approximate relationship

$$\frac{\partial J}{\partial (k_z z)} \approx - \frac{\partial J}{\partial (\omega t)}. \tag{16}$$

Subsequently, by using the above relationship and integrating by parts over time, equations (14) and (15) can be straightforwardly obtained.

For an electron beam represented by N_t discrete particles, the current density $\boldsymbol{J}$ can be easily written as

$$\boldsymbol{J}(\boldsymbol{x},t) = \frac{2\pi I_{\rm b}}{\omega}\sum_{j=1}^{N_t} W_j \delta(x-x_j)\,\delta(y-y_j) \times \delta(t-t_j)\,\frac{\boldsymbol{v}_j}{v_{zj}}, \tag{17}$$

where $I_{\rm b}$ is the beam current and carries a negative sign. The j-th particle passes through the cross section corresponding to the axial position z at time coordinate t_j and transverse coordinates x_j and y_j, at this moment v_{zj} and $\boldsymbol{v}_j$ are the axial and the vectorial velocities of the j-th particle, respectively.

In Eq. (17), W_j is the normalized weighting factor for the j-th particle, and the following constrain condition should be satisfied:

$$\sum_{j=1}^{N_t} W_j = 1. \tag{18}$$

When the electron momentum spread is considered, W_j takes the following form:

$$W_j = W_0 \exp\left[-(p_{zj}-p_{z0})^2/2\Delta p_z^2\right], \tag{19}$$

where p_{zj} is the j-th particle's axial momentum, p_{z0} is the average axial momentum, and Δp_z is the standard deviation of the momentum spread. The value of W_0 can be determined by using Eq. (18).

On the other hand, if the relation

$$\frac{{\rm d}\phi}{{\rm d}z} = k_z(z) - \sqrt{\omega^2/c^2 - k_x^2 + \kappa_0^2} \tag{20}$$

is defined, there will be an equation

$$\frac{\omega^2}{c^2} - k_x^2 - k_z^2 + \kappa_0^2 \cong -2k_z\frac{{\rm d}\phi}{{\rm d}z}, \tag{21}$$

where ϕ represents the accumulated phase offset produced from the deviation of k_z from the vacuum wave number during the beam–wave interaction.

After combining Eqs. (14), (15), and (17) and applying Eq. (21), we obtain two coupled first order differential equations

$$\frac{{\rm d}\phi}{{\rm d}z} = \frac{|I_{\rm b}|}{k_z A C_{mn}}\sum_{j=1}^{N_t} W_j \sin(k_x x_j) \times \left\{\kappa_0 \sinh\left[\kappa_0(b-y_j)\right]\cos\alpha - k_z\frac{v_{yj}}{v_{zj}}\cosh\left[\kappa_0(b-y_j)\right]\sin\alpha\right\}, \tag{22}$$

$$\frac{{\rm d}A}{{\rm d}z} = \frac{|I_{\rm b}|}{k_z C_{mn}}\sum_{j=1}^{N_t} W_j \sin(k_x x_j) \times \left\{\kappa_0 \sinh\left[\kappa_0(b-y_j)\right]\sin\alpha + k_z\frac{v_{yj}}{v_{zj}}\cosh\left[\kappa_0(b-y_j)\right]\cos\alpha\right\}, \tag{23}$$

where v_{yj} is the j-th particle's y-directional velocity.

The particle dynamics is governed by the relativistic equation of motion

$$\frac{{\rm d}\boldsymbol{p}}{{\rm d}z} = -\frac{e}{v_z}\left[\boldsymbol{E} + \boldsymbol{v}\times(B_0\hat{\boldsymbol{z}} + \boldsymbol{B})\right], \tag{24}$$

and the energy evolution is determined by the equation

$$\frac{{\rm d}\gamma}{{\rm d}z} = -\frac{e}{m_{\rm e}c^2 p_z}\boldsymbol{p}\cdot\boldsymbol{E}, \tag{25}$$

where e is the electron charge, $m_{\rm e}$ is the electron rest mass, and γ is the relativistic factor. The electromagnetic field in the waveguide is given by Eqs. (1)–(3).

At the initial position of the interaction structure, the amplitude corresponds to the power of the injected wave, and the wave number is set as the vacuum value in the cold-state waveguide. Though this simplified boundary condition excludes the backward and the evanescent waves, it is suitable for a steady-state amplifier model, in which the interested wave propagates at the same direction of the electron beam, and the related physical quantities can take the slowly varying assumption.

By solving Eqs. (22)–(25) through the Gill algorithm, the wave amplitude and the phase evolution in the rectangular Cerenkov maser can be determined with the forwardly streaming of the electrons. In succession, the wave number variation, the saturated power, the saturation length, the power growth rate, and the other interesting information can be further extracted from the calculated results.

3. Numerical results

In this section, a demonstrative example is given, in which the sheet electron beam interacts with the fundamental slow-wave mode EH_{10} of the dielectric loaded rectangular waveguide. A 150 kV, 10 A electron beam is injected, and is confined by a strong uniform magnetic field of 1 T. The tenuous sheet beam has a transverse dimension of 16 mm and propagates 1 mm above the dielectric surface. The rectangular

waveguide has a width of 20 mm, in which the thickness of the dielectric layer is 1 mm and the height of the vacuum regime is 4 mm. The relative permittivity of the dielectric layer is 5. In the following calculations, the above parameters will be used unless given explicitly.

The working frequency and the axial wave number at the initial position are separately chosen to be 40.01 GHz and 1322 m^{-1}, which correspond to the intersection point between the cold-state dispersion curve of the EH_{10} mode and the beam line. The input signal power is set at 10 W. Figure 2 shows the forward power evolution and the power growth rate along the axial coordinate. The wave power attains the saturated value of 95.01 kW at the axial position of 289.13 mm, where the signal gain is 39.78 dB. It can be observed that the power growth rate approaches zero at the axial position where the saturated power occurs. Figure 3 exhibits the variations of the axial wave number and the accumulated phase offset along the axial coordinate. The axial wave number first increases rapidly, then is almost unchanged. With the increase of the interaction length, the accumulated phase offset gradually becomes large. The normalized axial momentum evolutions of some representative particles are shown in Fig. 4, from which it can be noted that most particles lose their kinetic energies to the electromagnetic field at the saturation position.

The influence of the electron beam on the forward wave power evolution is displayed in Fig. 5. It can be found that the saturated power and the saturation length get higher and shorter respectively with the increase of the beam current. In this figure,

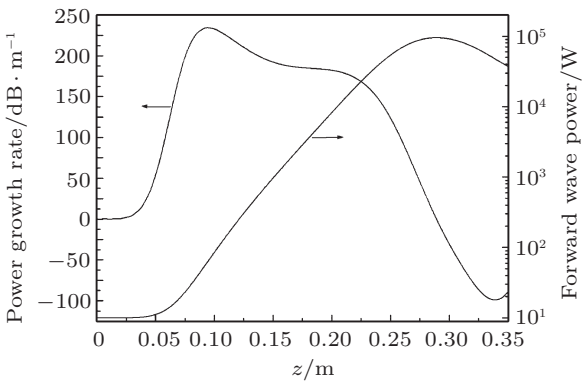


Fig. 2. Forward wave power and its power growth rate along the axial coordinate at 40.01 GHz for an ideal beam without momentum spread.

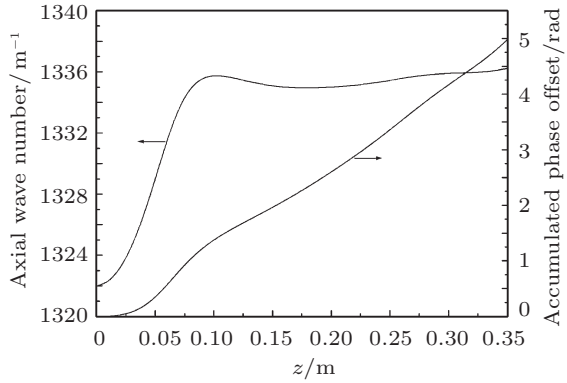


Fig. 3. Axial wave number and accumulated phase offset along the axial coordinate at 40.01 GHz for an ideal beam without momentum spread.

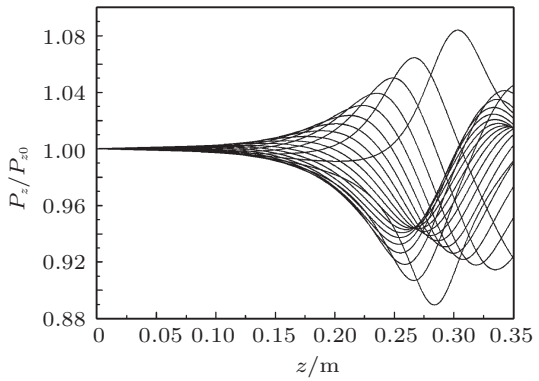


Fig. 4. The normalized axial momentum evolutions of some representative particles along the axial coordinate.

when the beam current is 15 A, the saturated power is 162.64 kW at the position of 263.62 mm; when the current is 5 A, the saturated power is 38.68 kW at 340.39 mm. The gap distance between the sheet beam and the dielectric surface has an evident influence on the beam–wave interaction. As shown in Fig. 6, a smaller gap can improve the saturated power after a shorter interaction length. For the gap distance of 0.8 mm, the saturated power is 108.39 kW at the position of 254.88 mm; for the case of 1.2 mm, the saturated power is 83.35 kW at 328.11 mm. The electron momentum spread $\Delta P_z/P_{z0}$ can obviously weaken the interaction, as demonstrated in Fig. 7. According to the forward wave power curves, the larger momentum spread of the electron beam will lower the saturated power and increase the saturation length. By comparing the case with the momentum spread of 0.02 with the ideal case without momentum spread, it can be observed that the saturated power decreases from 95.01 kW to 58.07 kW, and the saturation length correspondingly increases from 289.13 mm to 383.15 mm.

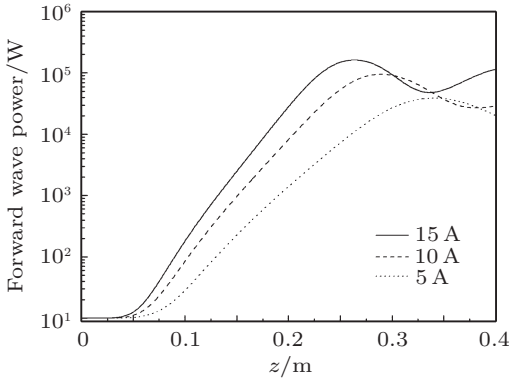


Fig. 5. The influence of beam current on the forward wave power evolution along the axial coordinate.

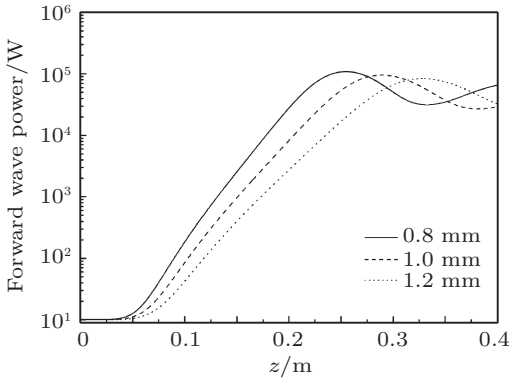


Fig. 6. The influence of the distance between the electron beam and the dielectric surface on the forward wave power evolution along the axial coordinate.

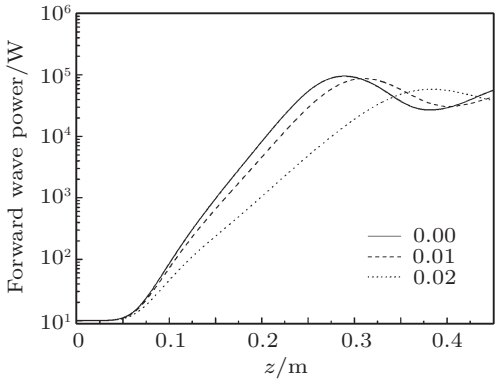


Fig. 7. The influence of electron momentum spread on the forward wave power evolution along the axial coordinate.

When the axial momentum spread of the electron beam, $\Delta P_z/P_{z0}$, changes from 0.0% to 2.25%, the relations between the saturated output power and the working frequency in the range of 37.8–42.0 GHz are shown in Fig. 8. It can be noted that the maximum saturated power decreases from 171.03 kW for the ideal beam without momentum spread to 74.53 kW for the beam with the momentum spread of 2.25%. Figure 9 exhibits the relations between the saturation length and the working frequency for the beams with different momentum spreads. For the ideal beam with a vanishing momentum spread, the curve of saturation length versus frequency has the widest flat region, namely, the saturation length keeps at about 300 mm in the regime of 38.36–40.87 GHz. When $\Delta P_z/P_{z0}$ increases to 2.25%, the flat segment of the curve shrinks evidently. According to the figure, the saturation length is approximate 406 mm in the range of 39.98-40.87 GHz. These results demonstrate that a beam with a lower momentum spread can realize more effective energy exchange and operate in a wider frequency range by using a shorter interaction length.

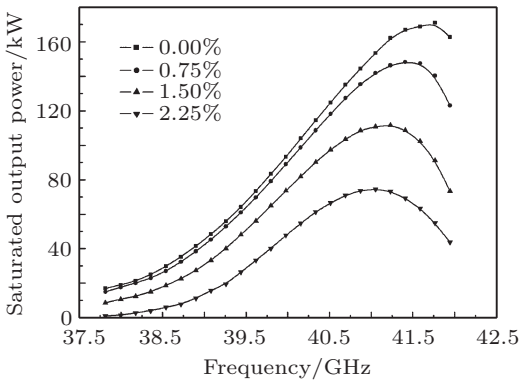


Fig. 8. Saturated output power versus the working frequency for the beams with different axial momentum spreads.

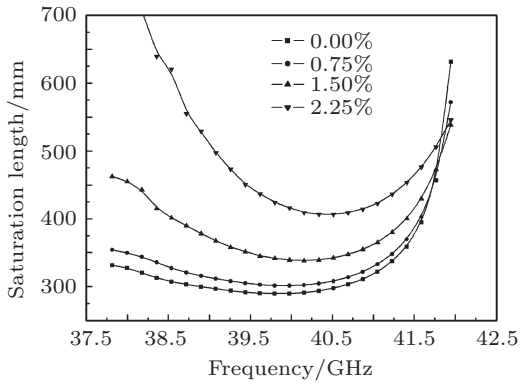


Fig. 9. Saturation length versus the working frequency for the beams with different axial momentum spreads.

To further verify the simplified nonlinear theory, another example is given in Fig. 10. The interaction structure is the same as that used in Fig. 2. Both the solid and the dash curves represent the forward wave power evolution along the axial coordinate, while the former is obtained from the simplified theory, and the latter is obtained by using the rigorous

method in Ref. [21]. It can be observed that these two curves show excellent agreement in the entire interaction length. The rigorous method predicts that the saturated power of 92.70 kW occurs at 289.61 mm, which is consistent with the result of the simplified method. The dotted curve in Fig. 10 represents the net power along the axial coordinate. For the amplifier model, the forward wave power is dominant in the net transmitted power, so the curves of them have the consistent tendency except at the beginning. At the initial phase, there exists a discrepancy between the net power and the forward wave power, which can be well explained by considering the launching loss in the traveling-wave interaction structure, namely, the forward amplifying wave dominates over the backward wave after traveling a finite distance. For a computer equipped with Intel Core i3 CPU, the running time of Fortran programs based on the simplified and the rigorous methods is about 20.5 s and 244.7 s, respectivley, which obviously shows that the the simplified theory is more efficient.

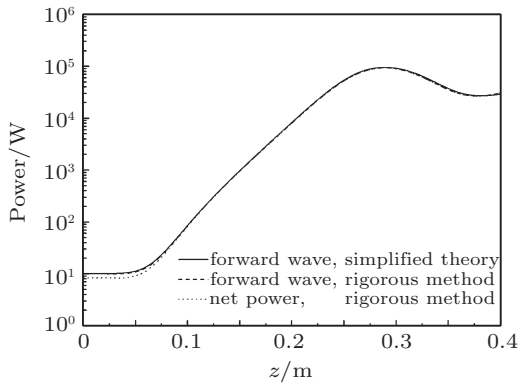


Fig. 10. The forward wave power and the net power evolution along the axial coordinate derived from the simplified theory and the rigorous method.

4. Summary

To investigate the beam–wave interaction in the dielectric loaded rectangular Cerenkov maser, a simplified nonlinear theory is proposed, in which the wave amplitude and the wave phase are determined by two coupled first-order differential equations. From the physical viewpoint, the beam–wave interaction will cause a complex shift in the axial wave number, the real and the imaginary parts of which reflect the wave phase and the wave amplitude variations, respectively. Through combining with the relativistic equation of motion and adopting the forward wave assumption, the interaction process can be determined in a single-pass calculation. By comparing with the result produced from the rigorous method, the deviation is observed in the beginning region, where the existence of the backward wave can lower the net transmitted power along the waveguide. The evolution curves of the forward wave power predicted by the two methods show excellent agreement, which indicates that the simplified nonlinear theory is accurate enough for the Cerenkov amplifier.

The simplified nonlinear theory has been used to study an illustrative example. The evolutions of the forward wave power, the growth rate, the axial wave number, and the accumulated phase offset can be given directly. The other interested information, for instance, the particle momentum, can also be extracted from the obtained results. The calculation demonstrates that the saturated power enhances and the saturation length shortens with a larger beam current, a smaller gap distance, and a lower momentum spread. When the focusing magnetic field is strong enough to sustain the beam propagation, it is noted that the intensity varying has no effect on the interaction, which is evident for the Cerenkov maser. The influence of the electron momentum spread on the relation between the saturated power (length) and the working frequency has also been obtained. It can be concluded that using a beam with a lower momentum spread can produce a higher saturated power in a wider frequency range by traveling over a shorter length. Due to its rapid and accurate characteristics, the developed simplified nonlinear theory can be effectively used to analyze and design dielectric loaded rectangular Cerenkov masers.

References

[1] Cerenkov P A 1934 *Doklady Akad. Nauk S.S.S.R.* **2** 451
[2] Ginzburg V L 1947 *Doklady Akad. Nauk S.S.S.R.* **56** 253
[3] Walsh J E, Marshall T C and Schlesinger S P 1977 *Phys. Fluids* **20** 709
[4] Felch K L, Busby K O, Layman R W, Kapilow D and Walsh J E 1981 *Appl. Phys. Lett.* **38** 601
[5] Laven S V, Branscum J, Golub J, Layman R and Walsh J 1982 *Appl. Phys. Lett.* **41** 408
[6] Garate E P, Moustaizis S, Buzzi J M, Rouille C and Lamain H 1986 *Appl. Phys. Lett.* **48** 1326
[7] Main W, Cherry R and Garate E 1989 *Appl. Phys. Lett.* **55** 1498
[8] Garate E, Kosai H, Evans K, Fisher A, Cherry R and Main W 1990 *Appl. Phys. Lett.* **56** 1092
[9] Kosai H, Garate E, Fisher A and Main W 1992 *IEEE Trans. Plasma Sci.* **20** 288

[10] Zhang T B, Marshall T C and Hirshfield J L 1998 *IEEE Trans. Plasma Sci.* **26** 787

[11] Lee C Y and Masuzaki M 1998 *Int. J. Infrared Millim. Waves* **19** 1255

[12] Cook A M, Tikhoplay R, Tochitsky S Y, Travish G, Williams O B and Rosenzweig J B 2009 *Phys. Rev. Lett.* **103** 095003

[13] Chang S R, Scharer J E and Booske J H 1992 *IEEE Trans. Plasma Sci.* **20** 293

[14] Walsh J E, Marshall T C, Mross M R and Schlesinger S P 1977 *IEEE Trans. Microwave Theory Tech.* **25** 561

[15] Uhm H S 1981 *J. Appl. Phys.* **52** 6533

[16] Shoucri M 1983 *Phys. Fluids* **26** 2271

[17] Garate E P and Walsh J E 1985 *IEEE Trans. Plasma Sci.* **13** 524

[18] Lee C Y, Yamashita R and Masuzaki M 1997 *Int. J. Infrared Millim. Waves* **18** 519

[19] Zhao D and Ding Y 2011 *Phys. Plasmas* **18** 093107

[20] Chen Y, Zhao D and Wang Y 2011 *Chin. Phys.* B **20** 108402

[21] Zhao D and Ding Y 2012 *Phys. Plasmas* **19** 024508

[22] Freund H P and Ganguly A K 1990 *Phys. Fluids* B **2** 2506